ARTICLE

Synthesis, characterization, and coating application of a highly conductive polyaniline-TiO_2 nanocomposite

Khaled A. Altannyhi, Elsayed M. Elnaggar, Badr A. Elsayed*, Mohamed M. Elsenety

Department of Chemistry, Faculty of Science, Al-Azhar University, Nasr City, Cairo, Egypt

Abstract

In the present work, synthesis, and characterization of a highly conductive polyaniline (PANI) doped with titanium dioxide (TiO_2) nanocomposite that allows static charges to flow through the floor and be safely grounded has been reported. The effect of different dopant concentrations on the conductivity and other properties of the PANI nanocomposite was investigated. Fourier Transform Infrared shows the characteristic vibrational bands of N−H, C−H, C═C, aromatic ring, and C−N at 3428, 2913, 1566, 1466, and 1294 cm^{-1} of the PANI and v(Ti−O) at 470 cm^{-1} of its composites. The lattice strain examined by Rietveld analysis of radiography diffraction data exhibits microstrain broadening of 7.3 due to local deformation of Ti and O atoms caused by interaction with PANI. Transmission electron microscopy analysis of the average size and distribution of PANI and its composite particles confirms the dispersion of TiO_2 in the PANI matrix, with diameters ranging from 2 to 22 nm and a median of 7 nm. The conductivity of PANI was increased with increasing the dopant of TiO_2 up to 10% (wt/wt) which was the optimal one exhibiting an excellent value of 33.93 S/cm, for the first time. PANI doped with 10% TiO_2 (PAT10) is a promising material for electronic manufacturing facilities, clean rooms, and other environments where static electricity can be a hazard. Highly conductive PAT10 nanocomposite as a floor coating effectively reduces electrostatic risks, providing both safety and durability.

Keywords: Conductive coating, Electrostatic discharge, Electrostatic discharge coating, Polyaniline/TiO_2 nanocomposites, Polyaniline

1. Introduction

Electrostatic discharge (ESD) is a natural physical phenomenon that can cause fires and explosions in industrial sites, leading to significant damages and losses.[1] ESD occurs when there is a sudden flow of electrons from one surface or human to another, creating a miniature spark that can damage electronics and cause data loss.[2,3] ESD is caused by the accumulation of static electricity between two surfaces due to friction, contact, and separation. Prevention and control of ESD are essential to avoid damages and losses.[4] A protective ground is necessary to provide a traceable path to the ground and prevent static from generating on people.[5] Antistatic floors and conductive materials can be used to prevent ESD and increase the electrical conductivity of epoxy compounds.[2,6] However, the creation of a layer of epoxy resin that contains conductive materials on the surface of a floor is widely used to prevent static electricity buildup and electromagnetic interference problems.[7] Conductive materials transfer charges from people's feet to the ground, effectively grounding the charges and removing them from the area. To increase the electrical conductivity of the epoxy matrix, electrically conductive materials such as copper, silver nanowires, carbon nanotubes or fibers (CNTs/CNFs), and conductive polymers (CPs) such as poly (3, 4-ethylenedioxythiophene) (PEDOT) and poly (pyrrole) (PPY) are added to the resin.[8,9] Materials used for ESD shielding can be classified into conductive and dispersive materials based on their resistance ranges. Conductive materials have a volumetric resistivity of less than 104 Ω/

Received 3 August 2023; revised 22 November 2023; accepted 29 November 2023.
Available online 30 April 2024

* Corresponding author at: Department of Chemistry, Faculty of Science, Al-Azhar University, Nasr City, Cairo, 11884, Egypt.
E-mail address: badrelsayed@azhar.edu.eg (B.A. Elsayed).

https://doi.org/10.62593/2090-2468.1001

cm^2 or a surface resistivity of less than 105 Ω/cm^2, while static dispersive materials have a volume resistivity of 104–1011 Ω/cm or a surface resistance of 105–1012 Ω/cm^2[5,10] Polyaniline (PANI) is a conductive polymer that is commonly used in coating systems, particularly in corrosion protection.[11] The conjugating system on PANI's backbone makes it a preferred conductive polymer in many applications. However, the conjugation alone is not sufficient to make the polymer conductive, and additional electrons or holes must be injected into the material.[12–16] PANI is also often combined with inorganic nanoparticles such as TiO_2 to create nanocomposites with unique properties, including different electrical, optical, and mechanical properties.[17–20] PANI is a p-type semiconductor with a band gap of 2.1 eV, and TiO_2 is a n-type semiconductor with a band gap of 3.13 eV.[21–23] Therefore, the two types of particles can be linked together by a p-n junction, and the resulting PANI/TiO_2 nanocomposite can provide barriers to electronic migration.[11,24–26]

This study investigates the effect of dopant concentrations on the conductivity and properties of a PANI nanocomposite. The highly conductive PAT10 (PANI/TiO_2) nanocomposite was used in epoxy resin formulations and the antistatic properties which has potential applications as a floor coating in environments where static electricity can be a hazard, such as electronic manufacturing facilities and clean rooms. This work has a significant help to develop effective methods to prevent and control ESD, thereby reducing damages and losses in industrial sites.

2. Experimental

2.1. Material

Aniline, Ammonium persulfate (APS), and TiO_2 with an average particle size of 150 nm were used as a pigment in this study. Calcium carbonate with an average particle size of 200 nm was used as an extender. The dispersant Alkylammonium salt of a high molecular-weight copolymer with a molecular weight of 5000 g/mol was supplied from Witting and Disspers (W and D) BYK 9076 (Germany). An industrial grade Xylene was employed as a pollutant. Epoxy resin EPOTEC YD 128 (Germany), Epoxy hardener ANCAMINE 1618 as Curing Agent (Germany), reactive diluent EPOTEC RD 108 (Germany), Surface Additive BYK 306 (Germany), and antifoaming agent BYK A 530 (Germany), Leveling agent BYK 320 (Germany), HCl (33%), Methanol, and Acetone.

2.2. Synthesis of polyaniline

The template-free method was used to prepare the PANI nanostructure as in the previous article[27] but with the molar ratio of the oxidant increased to 1.25 of the monomer ratio to reduce the presence of unpolymerized aniline and to obtain the highest yield of PANI and reached 92%, compared 60% of the previous study.[28] Aniline hydrochloride monomer was prepared by mixing 1 mol of aniline with 1 mol of HCl in an aqueous solution. The solution was stirred for 1 h to ensure the formation of a homogeneous solution of aniline–HCl. The preweighted APS was dissolved in deionized water and slowly added to the reaction mixture in a dropwise manner under vigorous stirring using a magnetic stirrer at room temperature (22 °C)for 2 h. Then, the mixture was allowed to polymerize by stirring for 24 h. The color of the solution gradually changed from white to green. Then, a dark green precipitate is obtained by filtering the mixture. The precipitate was washed repeatedly with distilled water, dilute hydrochloric acid, methanol, and acetone to remove any unreacted regents and left to dry at room temperature. PANI hydrochloride powder was finally obtained by slight grinding.

2.3. Synthesis of polyaniline/TiO_2 composites

The synthesis of PANI-TiO_2 composites involved an *in situ* chemical polymerization method. A solution of aniline hydrochloride (6.5 g PANI + 6 ml HCl (33% v/v)+100 ml deionized water) served as the base for the synthesis. TiO_2 was introduced at varying concentrations (2%, 4%, 6%, 10%, 12%, and 14% by weight of aniline hydrochloride). To achieve a uniform dispersion of TiO_2 in the monomer solution, vigorous stirring was carried out for 30 min. Subsequently, a solution containing 14.3 g of ammonium persulfate in 100 ml of 0.1 N HCl was added to initiate the polymerization process. The yield percentage of the polymerization process ranged from 88% to 90%, with an increase in the ratio of incorporated TiO_2.

2.4. Preparation of coating formulations

A 40 g PANI composite TiO_2 10% (PAT10) (selected for coating formulation due to the highest conductivity) was added to a portion of 100 g epoxy resin containing the 1 g BYK 9076 wetting and dispersing agent. The ingredients are mixed well with a mechanical stirrer until a homogeneous

slurry is obtained. Then the conventional additives such as an anti-foaming agent 2 g BYKA 530, leveling agent 0.8 g BYK 306 and BYK 320, and 57 g $CaCO_3$ were added to the mixture while stirring continuously for 10 min these component A was mixed with Component B of 50 g ANCAMINE 1618 by mixed ratio 100:25% and was applied to the concrete substrate for evaluation. Note that: the PAT10 was added in proportions of 0, 10, 20, 30, and 40% of the total composition and was applied to the concrete substrate for optimization and evaluation.

3. Result and discussion

3.1. FTIR analysis

FTIR spectroscopy was used to characterize the chemical structure and functional groups of PANI and PAT10 materials. The FTIR spectrum of PANI as shown in Fig. 1, typically exhibits strong stretching vibrational bands of N–H, C–H, C=C, aromatic ring, and C–N at 3428, 2913, 1566, 1466, and 1294 cm^{-1}, respectively.[24,29] Moreover, the bands observed at 1132, and 792 cm^{-1} are corresponding to aromatic C–H in the plane and out-of-plane bending vibrational modes, respectively.

In addition, the PANI-doped TiO_2 (PAT10) shows characteristic absorption bands corresponding to the functional groups present in both the PANI and the dopant. The most characteristic absorption bands in the FTIR spectra of TiO_2 are typically seen in the range of 400–1000 cm^{-1} and it has been reported around 450 cm^{-1}.[24] As a result of first derivatives of IR spectrum, the vibrational band at 470 cm^{-1} in the of PAT10 is related to the Ti–O

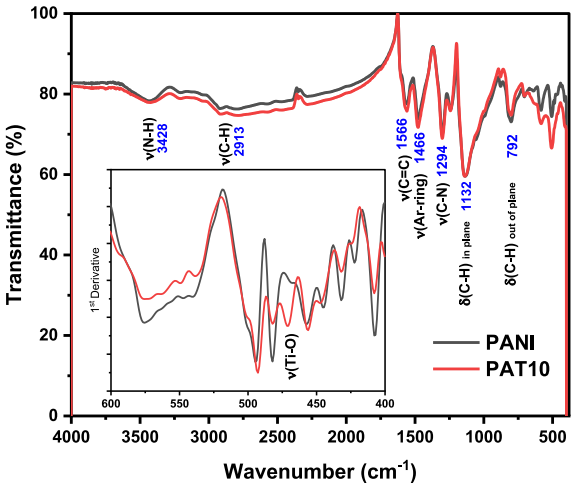

Fig. 1. Fourier transform infrared of polyaniline and PAT10, (First derivatives of polyaniline and PAT10 spectra).

stretching vibration. In addition, the absorption bands in the range between 400 and 1000 cm^{-1} were shifted to a lower wavenumber by about 2 cm^{-1}. This finding confirms the presence of the dopant of TiO_2 as physically interacted with PANI.

3.2. Structure analysis

XRD technique was used to determine the structural properties and crystal structure of PANI and PAT10 composite. Fig. 2a illustrates the XRD pattern of PANI in comparison with the PAT10. The results show the amorphous or semi crystalline structure of PANI and formed relatively weak peaks at 2 θ around 20.03 and 25.36° caused by the polymer chains being arranged parallel and closely spaced from one another. The XRD pattern of PANI doped with 10% TiO_2 (PAT10) shows diffraction peaks corresponding to the crystal structures of both the PANI and the dopant. The XRD pattern of PAT10 shows the characteristic peaks of the anatase phase of TiO_2 (JCPDS PDF#021-1276) at 2 θ equal to 27.44°, 36.09°, 39.19°, 41.23°, 54.05°, 56.64°, 62.74°, 64.04°, 65.48°, and 69.01° which corresponding to (110), (101), (111), (211), (220), (002), (310), (221), and (301), respectively.[29,30] The relative intensities and positions of the diffraction peaks of PAT10 were further analyzed using Rietveld refinement[31–35] as shown in Fig. 2b. The tetragonal crystal system of TiO_2 (Space group: P42/mm #136, a: 4.5933 Å, c: 2.9592) was used as initial crystallographic parameters for Rietveld analysis. The diffraction peaks of PAT10 were well-indexed and matched with the literature and no extra peaks of impurities were found. However, the lattice parameter 'a' was a little increased to 4.5946 (3) Å by about 0.0013 Å. In contrast, the lattice parameter 'c' was a little decreased to 2.9588(2) Å by about 0.0006 Å, which is not significant chemical interaction could occur. Overall, these results suggest a physical interaction (Van-der-Waals Forces) between TiO_2 and PANI. Furthermore, a size-strain plot based on the Williamson-Hall method was used to assess crystal size and lattice strains as shown in Fig. 2c.

The PAT10 exhibits microstrain broadening of 7.3, and it would be attributed to a slight local deformation of Ti and O atoms caused by interaction with PANI. Meanwhile, the crystallite size of PAT10 was equal to 38.46 nm, which confirms the nanocomposite formation of PANI TiO_2 doped materials.

3.3. Morphology analysis

Scan electron microscopy (SEM), transmission electron microscopy (TEM) and statistical analysis

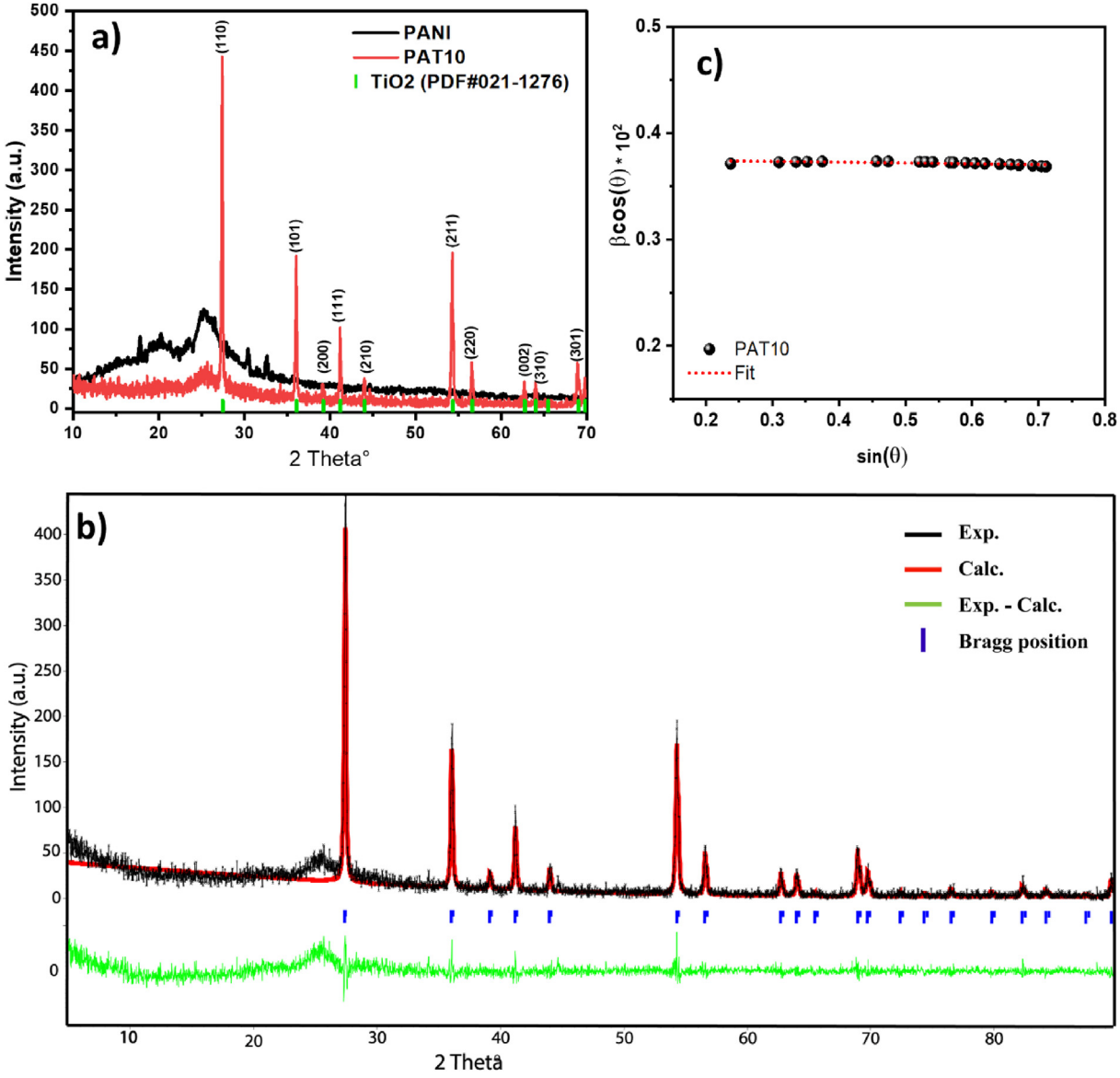

Fig. 2. XRD patterns of polyaniline and PAT10 (a); Rietveld refinement of PAT10 (b); and size-strain plot of PAT10 based on the Williamson-Hall method (c).

were used to investigate the shape and morphology of the PAT10 composite at the nanoscale. It worth to mention, high-conductive materials tend to accumulate electrons from the SEM beam, leading to charging effects. This can cause distortion and artifacts in the images, making it difficult to obtain accurate information about the sample's surface for both PANI and PAT10 as shown in Fig. 3a–d. However, the TEM image of the PAT10, and PANI composites as shown in Fig. 3b–e shows that the PANI is distributed throughout the TiO_2 matrix in the form of nano, spherical-like structures in which PANI is shown as a core covered by a TiO_2 layer.

The degree of dispersion of TiO_2 in the PANI matrix can be statistically determined by measuring the average size and distribution of the PAT10 particles (diameters in the range of 2–22 nm with a median of 7 nm) compare with (diameters in the range of 5–30 nm with a median of 18 nm) of PANI, which confirm PAT10 nanocomposite as shown in Fig. 3c–f.

3.4. Optoelectronic analysis

The electronic properties of PANI and PAT10 were investigated using diffuse reflectance spectroscopy, at room temperature. It is well known that diffuse reflectance of a material is a measure of how much light is reflected by the surface of the material when it is illuminated by a light source.[36] Thus, the

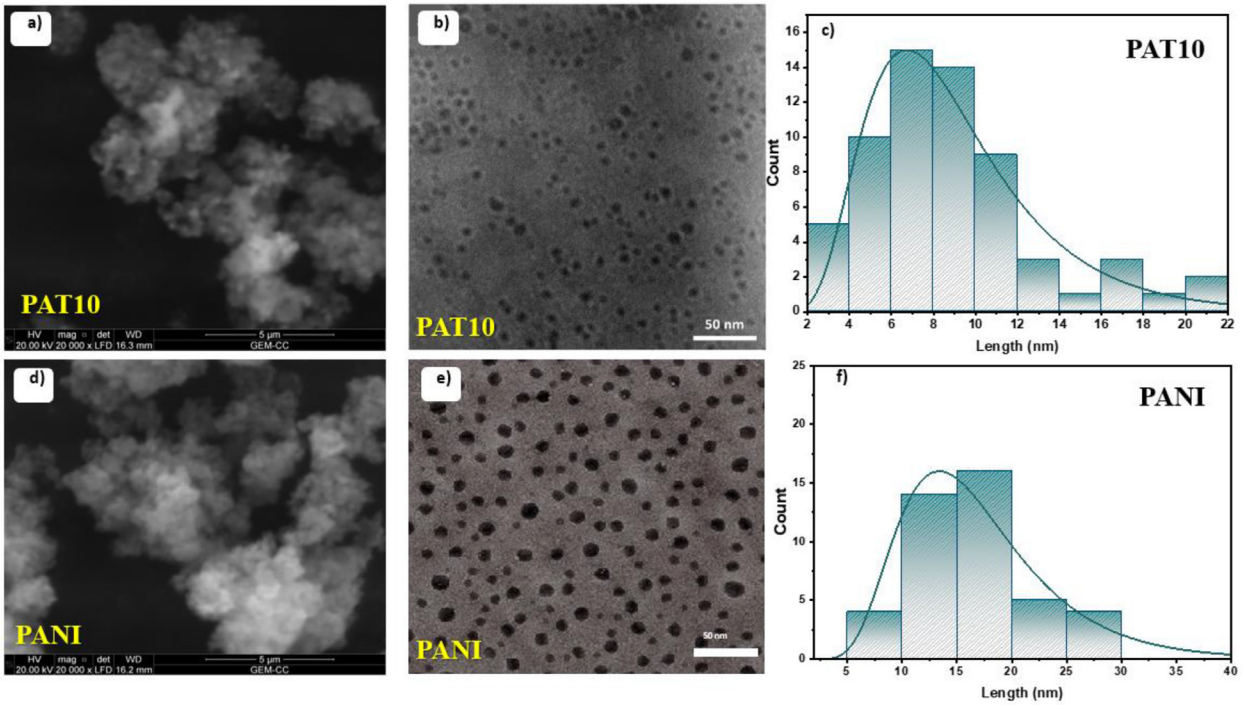

Fig. 3. Morphology analysis of PAT10 including Scan electron microscopy (a); transmission electron microscopy image (b); statistical distribution nanoparticles (c); and for the PAT10: Scan electron microscopy (d); transmission electron microscopy image (e); statistical distribution nanoparticles (f).

diffuse reflectance of PANI can vary depending on the specific properties of the material, such as the degree of crystallinity and the presence of impurities or doped TiO_2. In general, PANI is known to have a relatively low diffuse reflectance, which is typical of many semiconducting materials. This means that a relatively small fraction of the light that is incident on the surface of the material is reflected, and most of the light is absorbed. Fig. 4 depicts the Kubelka-Munk reflectance spectra of PANI in comparison with PAT10 materials. The x-axis intercept of a linear extrapolation of the low energy region of each curve was used to calculate the indirect bandgap (Eg) values.

It worth to mention, the pristine TiO_2 nanoparticles band gap was reported 3.2 eV in literatures. However, the band gap of PANI TiO_2 composite could calculated based on the higher absorption band of the curve which equal 2.9 eV, and that is lower than pristine TiO_2.[37] In addition the results show a clear significant red shift up to 1.21 eV compared with nondoped PANI materials which could be a result of interstitial state or excitons due to formation of PANI TiO_2 composite.[24] This finding suggests that PAT10 exhibited a bit stronger response in the visible light range than PANI, which could boost conductivity efficiency in different applications.

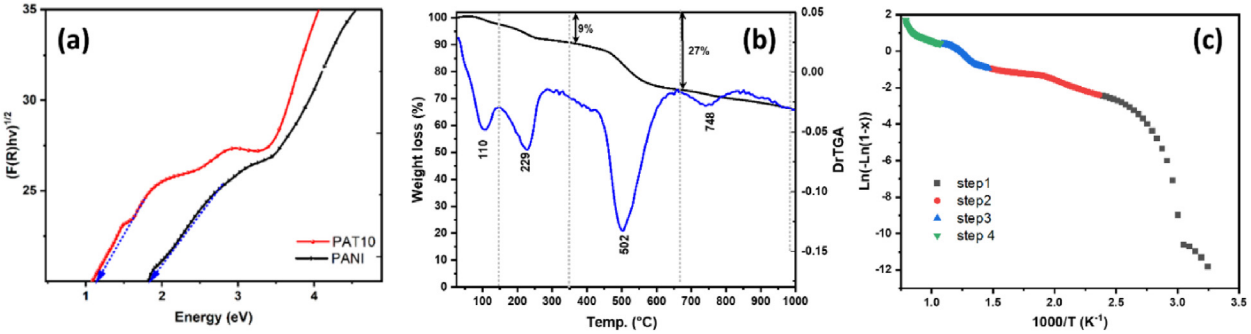

Fig. 4. (a) The optical band gap energy of polyaniline and PAT10; (b) TGA and DrTGA of PAT10; (c)Plot of ln[-ln(1-x)] versus 1000/T of four steps decomposition (b).

However, it's been reported that PANI doped TiO_2 samples can have a higher diffuse reflectance than pure PANI samples due to the increased crystalline structure of PANI in the presence of TiO_2 as discussed above in the XRD section.

3.5. TGA and thermodynamic analysis

Thermal gravimetric analysis (TGA) conducted in this study was used to measure the weight loss of the material as a function of temperature. PAT10 nanocomposite was analyzed through TGA/DrTGA (differential thermal gravimetric analysis) with a heating rate of 10 °C min^{-1} in the range of 30–1000 °C, under N_2 gas, to show the thermal degradation of PANI-doped TiO_2 and better understand the mechanism of this process as shown in Fig. 4b and c. Thus, PAT10 undergoes thermal degradation at temperatures 50–145 °C, resulting in a weight loss of around 3% due to dehydration and removal of adsorbed water molecules on the surface of PAT10 nanoparticles. The result accords with the evaporation of moisture trapped inside the polymer or bound to the polymer backbone, as demonstrated by the degradation stage in the second step (229–350C).[29,38] In addition, the thermal degradation of PAT10 is breaking down the polymer material when exposed to high temperatures greater than 500 °C weight loss of 27% from the initial weight. TGA can be used to determine the kinetics and thermodynamic parameters of PANI-doped TiO_2.[39] Moreover, the Coats-Redfern model is a method used to analyze the TGA data, which allows the determination of various thermodynamic parameters such as activation energy, entropy, enthalpy, and Gibbs free energy, which are recorded in Table S1 (in the supplementary file). The activation energy is an important parameter that represents the energy required to initiate the degradation process. The results of this study show that the activation energy increases as the temperature increases, indicating that it becomes harder to initiate the degradation process at higher temperatures. The activation energy of 28011 J/mol at 145 °C and 34943 J/mol at 650 °C, are relatively high values, which suggest that the thermal degradation process is difficult to initiate and it requires a lot of energy to start. This can be an indication that the PAT10 has higher thermal stability at 650 °C than at 145 °C. Even that the PANI doped with 10% TiO_2 (PAT10) give a relatively good stability lower than 100 °C which more than enough for our target application. The entropy of the system is a measure of the disorder or randomness of the system. The results of this study show that the entropy of the system decreases as the temperature increases, indicating that the system becomes more ordered as the temperature increases. The entropy values of −245 J/mol K and −266 J/mol K at 145 and 650 °C, respectively, suggest that the thermal degradation process leads to a decrease in disorder in the system. Indeed this behavior could be associated with an increase in crystallinity and ordered arrangement of TiO_2 particles within the polymeric matrix. The thermal degradation process might influence the arrangement of these components, leading to changes in their crystalline structures.[40] The enthalpy is a measure of the heat absorbed or released during the degradation process. The results of this study show that the enthalpy increases as the temperature increases, indicating that more heat is absorbed as the temperature increases. The enthalpy values of 24827 J/mol and 28499 J/mol at 145 and 650 °C, respectively, suggest that the thermal degradation process absorbs a lot of heat. This can be an indication that the polymer has a high heat of combustion. Finally, Gibbs's free energy is a measure of the energy available to do work. The results of this study show that the Gibbs free energy increases as the temperature increases, indicating that the energy available to do work also increases as the temperature increases. The Gibbs free energy values of 119007 J/mol at 145 °C and 235091 J/mol at 650 °C, suggest that the thermal degradation process releases a lot of energy, which can be used to do work. Overall, the results suggest that the PANI-doped TiO_2 is thermally stable, releases a lot of energy when degraded, and has a high heat of combustion.

3.6. Conductivity measurements of PANI and PANI/TiO_2

Conductivity is a crucial property of materials. It was determined for PANI and its composites with TiO_2 through the four-probe technique as shown in Figure (a). The results revealed that the pure PANI exhibited a conductivity of 9.12 S/cm, a value that was subject to improvement through the incorporation of TiO_2.

The conductivities of PANI doped with TiO_2 were studied with different weight ratios, namely 2%, 4%, 6%, 10%, 12%, and 14%. The results showed a remarkable increase in conductivity with increasing TiO_2 content up to 10%, with values of 25.33, 26.56, 27.43, 33.93, 19.09, and 13.36 S/cm, respectively. It was intriguing to observe the influence of TiO_2 on the conductivity of PANI. The values of conductivity observed with different ratios of TiO_2 showed a fluctuation, with the significant conductivity of 33.93 S/cm observed with 10% TiO_2 content (Table S2 (in the supplementary file)). However, the

conductivity showed a decline with a further increase in TiO_2 content, suggesting a delicate balance between the two components in optimizing the conductivity. Furthermore, it is interesting to note that the increase in conductivity with the increase of TiO_2 content up to 10%. This could be attributed to several factors related to the incorporation of TiO_2 nanoparticles. TiO_2 nanoparticles can act as electron acceptors and donors, facilitating charge transfer between the polymer chains. This increased charge carrier mobility can enhance the overall conductivity of the composite.[24,41,47] Also, the combination of PANI and TiO_2 may exhibit synergistic effects, where the properties of the composite are greater than the sum of its individual components. This synergy can arise from the complementary electronic properties of the two materials.[11,26,42]

3.7. Antistatic performance

Epoxy coating is a well-known insulation coating, with very high surface resistivity. When PAT10 is incorporated with 40, 30, 20, and 10 wt% of Epoxy, the EP-PAT10 presented good electrical properties. Table 1 shows the measured surface resistivity and conductivity which indicate that the EP-PAT10 can dissipate a charge by both surface conduction (according to ANSI/EIA-541 standard). Compared with pure Epoxy without PAT 10.

The basis of the antistatic coating process is the free transfer of electrostatic charges along with the polymer matrix within the coating system, causing the film to become electrostatically dispersive. Numerous elements, including the type of epoxy resin, the form, the quantity, and the dispersion of CPs, as well as the characteristics of additives, affect a coating's antistatic properties. The term 'percolation threshold' refers to the minimum volumetric concentration of CPs that must be present to create an electrostatic conductive network.[43] Thus, and according to the obtained antistatic results, we can say that the percent of 20% will be considered the beginning of the percolation threshold point for the present formulation as reported in.[43]

Table 1. PAT 10 Add ratio with Surface Resistivity and Conductivity of Epoxy.

PAT 10 Add ratio	Surface Resistivity Ω/cm^2	Conductivity S.cm^2
EP- Blank	1.9×10^{13}	526.315×10^{-16}
10% PAT 10	18.44×10^{11}	542.29×10^{-15}
20% PAT 10	5.42×10^{9}	184.50×10^{-12}
30% PAT 10	0.3×10^{8}	333.3×10^{-10}
40% PAT 10	0.1×10^{6}	1×10^{-5}

3.8. Measurement of surface humidity

The results obtained with the Frequency-based Moisture Meter (FFM) 100 device on a concrete cube, an epoxy-coated concrete cube, and an epoxy-PAT10 coated concrete cube showed results of 52, 48, and 28% moisture. These results show a very sharp decrease in moisture content in a coating containing PAT10 compared with the epoxy-only coating and the uncoated concrete cube. This sharp decrease is attributed to the supper hydrophobicity of the PANI/TiO_2-containing Epoxy coating.[44] The drastic hydrophobicity can be explained as follows: Despite the relative hydrophilicity of epoxy resin, PANI as well as titanium oxide individually, the mixing of these three compounds results in hydrogen bonds between the active sites represented by the oxygen atom in the epoxy resin, the hydrogen atom in the doped acid in PANI and the oxygen atom in TiO_2. This association results in the absence of active sites in the Epoxy-PANI/TiO_2 capable of making hydrogen bonds with water molecules in moisture.

3.9. Measurement of adhesion

As mentioned above, the load is increasingly applied until the dolly is pulled off. The force required to pull the dolly off or the force the dolly withstood is recorded as the adhesion force. Failure occurs along the weakest plane within the system comprised of the dolly, adhesive, coating system, and substrate, and will be exposed by the fracture surface. The result of the adhesion strength test was completely different from the usual one, as the paint consisting of epoxy with PANI oxide - titanium showed a very high adhesion strength, which resulted in breaking the upper layers of the concrete cube without separating the paint layer, which means infinite adhesion between the paint and the concrete surface. Error! Reference source not found. (b) shows the degree of adhesion of the paint material and the refraction of the cube without separation of the paint layer.

3.10. Abrasion resistance

Table S3 (in the supplementary file), and Fig. 5c show the relationship between the number of cycles and the lost weight of the tapered rotary scraper, which was performed by ASTM D 4060. Although the pristine epoxy showed a weight loss of 88 mg, we note the Epoxy-PAT10 20%, lost only 28 mg after 500 cycles, which means a superior improvement in abrasion resistance. It is generally considered an

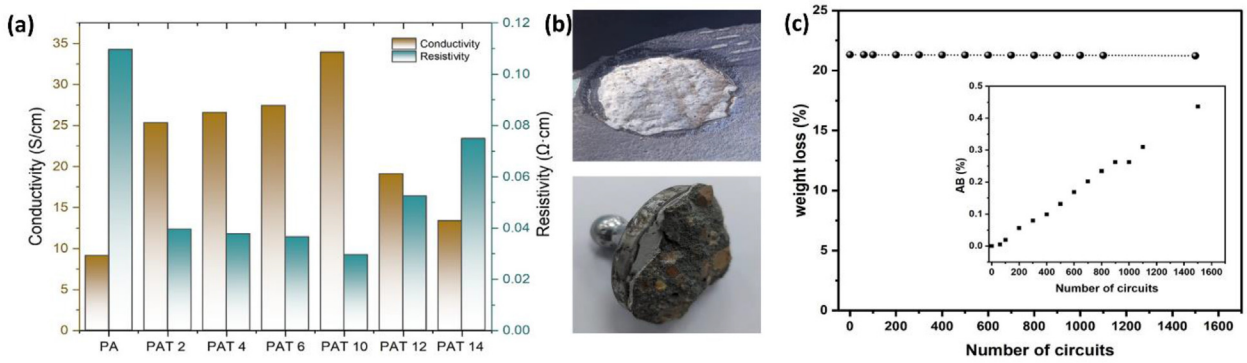

Fig. 5. (a) Conductivity and Resistivity of Polyaniline doped TiO_2 through the four-probe technique; (b) Dolly off the test on the coating (epoxy/PAT10 20%) surface after the test; (c) Relationship between the number of cycles and the lost weight of the tapered rotary scraper.

excellent performance result. To our knowledge, no one has been able to achieve this result previously. This means that the Epoxy coating with PAT 10 was able to withstand a great deal of wear without showing signs of wear or deterioration. The positive direction in the abrasion resistance may be attributed to the incorporation of the nano PANI-TiO_2 particles into the epoxy coating which increased the interface surface interaction between the nano-sized PANI-TiO_2 particles and epoxy coating base matrix providing more compact, more smooth, and less abraded film as compared with the coating without PANI-TiO_2 particles.[45] Investigations using potentiodynamic polarization measurements, cure durability, ultraviolet immovability, and abrasion resistance of polyamine-cured ilmenite epoxy coating for oil and gas storage steel tanks in the petroleum sector were studied by Al-Sabagh and colleagues that show the improvement in the abrasion resistance character may be described as previously,[46] the well-dispersion of composite particles tend to occupy holidays such as pinholes and voids in the thin-film coating and serve as the bridges in the interconnected matrix, causing a reduction in the total free volume and an enhancement in cross-linking density of the cured film. As such, the cured epoxy ilmenite coating has reduced chain segmental motions and improved stiffness.

3.11. Conclusions

In conclusion, the study reports the synthesis and characterization of highly conductive PANI doped with TiO_2 (PAT10) nanocomposite and using it in Epoxy coating formulation for ESD applications. The conductivity of PANI was found to increase with increasing the dopant up to 10% (wt/wt), resulting in an excellent value of 33.93 S/cm. TEM analysis showed that the particles of PAT10 have diameters ranging from 2 to 22 nm and a median of 7 nm. The incorporation of nano PANI-TiO2 particles into the epoxy coating (Epoxy-PAT10 20%) results in a remarkable enhancement of abrasion resistance, demonstrated by a weight loss of only 28 mg after 500 cycles, compared with 88 mg for the pristine epoxy. We suggest that PAT10 is a promising material for environments where static electricity can be a hazard and that it could be used as ESD coatings as like as Intensive care rooms in hospitals, floors of chemical and flammable materials stores, roofs and floors of ships and oil tankers … etc. The percentage of adding PAT10 to the epoxy paint is a 20% percolation threshold, which can then overcome the resistivity of the epoxy coating and turn it into a dissipative coating. It is also possible to add larger amounts of up to 40% if more conductivity is desirable.

Authors contributions

Khaled A. Altannyhi: Conceptualization, Data curation, Investigation, coding, Formal analysis, Methodology, Writing—original draft, Formal analysis, Supervision. Elsayed M. Elnaggar/ Mohamed M. Elsenety Data curation, Formal analysis, Methodology, Investigation, Writing—original draft, Investigation, Methodology. Badr A. Elsayed.: Writing—review & editing, Supervision.

Conflicts of interest

None declared.

Acknowledgements

Authors acknowledge support from the Department of Chemistry, Faculty of Science, Al-Azhar University.

References

1. Greason WD. *Electrostatic discharge in electronics, n.d.*; 1992. https://scholar.google.com/scholar?hl=en&as_sdt=0%2C5&q=Greason+WD+%281992%29+Electrostatic+discharge+in+electronics.+Research+Studies+Press+%28Taunton%29%2C+New+York.%5D&btnG=. (accessed March 12, 2023).
2. Chen ZH, Tang Y, Yu F, Chen JH, Chen HH. Preparation of light color antistatic and anticorrosive waterborne epoxy coating for oil tanks. *J Coating Technol Res*. 2008;5:259–269.
3. Galembeck F, Burgo TAL. *Chemical Electrostatics: New Ideas on Electrostatic Charging: Mechanisms and Consequences*. 2017: 1–230.
4. Rosner RB. Conductive materials for bsd applications: an overview. *IEEE Trans Device Mater Reliab*. 2001;1:9–16.
5. No Title, (n.d) (a). https://staticworx.com/faq/adding-static-dissipative-conductive-properties-flooring/.
6. Wu L, Ge Y, Zhang L, Yu D, Wu M, Ni H. Enhanced electrical conductivity and competent mechanical properties of polyaniline/polyacrylate (PANI/PA) composites for antistatic finishing prepared at the aid of polymeric stabilizer. *Prog Org Coating*. 2018;125:99–108.
7. Freitas FS, Gonçalves AS, De Morais A, Benedetti JE, Nogueira AF. Graphene-like MoS2 as a low-cost counter electrode material for dye-sensitized solar cells. In: *This Journal Is © NanoGe Journal on Energy and Sustainability*. 2012: 11002–11003.
8. Krushnamurty K, Rini M, Srikanth I, et al. Conducting polymer coated graphene oxide reinforced C-epoxy composites for enhanced electrical conduction. *Compos Part A Appl Sci Manuf*. 2016;80:237–243.
9. Singh NP, Gupta VK, Singh AP. Graphene and carbon nanotube reinforced epoxy nanocomposites: a review. *Polymer (Guildf)*. 2019;180:121724.
10. No Title, (n.d) (b). https://widaco.net/product-category/flooring/esd-floor/?gclid=Cj0KCQiAvqGcBhCJARIsAFQ5ke5Gn0x7ko-zAtpXadUq0Xdf-1dXdbCvtr2mrqua9uxTrGA-42PECuMaAqK7EALw_wcB.
11. Gao F, Mu J, Bi Z, Wang S, Li Z. Recent advances of polyaniline composites in anticorrosive coatings: a review. *Prog Org Coating*. 2021;151:106071.
12. Koul S, Chandra R, Dhawan SK. Conducting polyaniline composite for ESD and EMI at 101 GHz. *Polymer (Guildf)*. 2000;41:9305–9310.
13. Barkoula NM, Alcock B, Cabrera NO, Peijs T. Poly(Phosphate) and mineral filler magnesium hydroxide in combination with graphene. *Polym Polym Compos*. 2008;16:101–113.
14. Belaabed B, Lamouri S, Naar N, Bourson P, Hamady SOS. Polyaniline-doped benzene sulfonic acid/epoxy resin composites: structural, morphological, thermal and dielectric behaviors. *Polym J*. 2010;42:546–554.
15. Hassan S, Baker AG, Jafaar H. A.C electrical conductivity for polyaniline prepered in different acidic medium. *Int J Basic Appl Sci*. 2012;1:338–348.
16. Nguyen AS, Nguyen TD, Thai TT, et al. Synthesis of conducting PANi/SiO2 nanocomposites and their effect on electrical and mechanical properties of antistatic waterborne epoxy coating. *J Coating Technol Res*. 2020;17:361–370.
17. Su SJ, Kuramoto N. Processable polyaniline-titanium dioxide nanocomposites: effect of titanium dioxide on the conductivity. *Synth Met*. 2000;114:147–153.
18. Mohamed WAA, Fahmy A, Helal A, et al. Degradation of local Brilliant Blue R dye in presence of polyvinylidene fluoride/MWCNs/TiO2 as photocatalysts and plasma discharge. *J Environ Chem Eng*. 2022:10.
19. Mohamed WAA, Abd El-Gawad HH, Handal HT, et al. TiO2 quantum dots: energy consumption cost,germination, and phytotoxicity studies, recycling photo and solar catalytic processes of reactive yellow 145 dye and natural industrial wastewater. *Adv Powder Technol*. 2023:34.
20. Mohamed WAA, Abd El-Gawad HH, Handal HT, et al. Study of phytotoxicity, remarkable photocatalytic activity, recycling process and energy consumption cost of TiO2 quantum dots photocatalyst for photodegradation of Coomassie brilliant blue R dye. *Opt Mater*. 2023:137.
21. Elsenety MM, Stergiou A, Sygellou L, Tagmatarchis N, Balis N, Falaras P. Boosting perovskite nanomorphology and charge transport properties via a functional D–π-A organic layer at the absorber/hole transporter interface. *Nanoscale*. 2020;12:15137–15149.
22. Elsenety MM, Christopoulos E, Falaras P. Passivation engineering using ultra-hydrophobic D-π-A organic dye with machine learning insights for efficient and stable perovskite solar cells. *Solar RRL*. 2023;7:2201016.
23. Rezk H, Elsenety MM, Ferahtia S, Falaras P, Zaky AA. A novel parameter identification strategy based on COOT optimizer applied to a three-diode model of triple cation perovskite solar cells. *Neural Comput Appl*. 2023:1–23, 2023.
24. Nosrati R, Olad A, Najjari H. Study of the effect of TiO2/polyaniline nanocomposite on the self-cleaning property of polyacrylic latex coating. *Surf Coat Technol*. 2017;316: 199–209.
25. Hashemi Monfared A, Jamshidi M. Synthesis of polyaniline/titanium dioxide nanocomposite (PAni/TiO2) and its application as photocatalyst in acrylic pseudo paint for benzene removal under UV/VIS lights. *Prog Org Coating*. 2019;136: 105257.
26. Sonker RK, Yadav BC, Gupta V, Tomar M. Fabrication and characterization of ZnO-TiO 2 -PANI (ZTP) micro/nanoballs for the detection of flammable and toxic gases. *J Hazard Mater*. 2019:126–137.
27. Elnaggar EM, Kabel KI, Farag AA, Al-Gamal AG. Comparative study on doping of polyaniline with graphene and multi-walled carbon nanotubes. *J Nanostructure Chem*. 2017;7:75–83.
28. Stejskal J, Gilbert RG. Polyaniline. Preparation of a conducting polymer (IUPAC technical report). *Pure Appl Chem*. 2002;74:857–867.
29. Rajakani P, Vedhi C. Electrocatalytic properties of polyaniline–TiO2 nanocomposites. *Int J Ind Chem*. 2015;6: 247–259.
30. Hamad H, Elsenety MM, Sadik W, et al. The superior photocatalytic performance and DFT insights of S-scheme CuO@TiO2 heterojunction composites for simultaneous degradation of organics. *Sci Rep*. 2022;12:1–20.
31. Elsenety MM, Kaltzoglou A, Antoniadou M, Koutselas I, Kontos AG, Falaras P. Synthesis, characterization and use of highly stable trimethyl sulfonium tin(IV) halide defect perovskites in dye sensitized solar cells. *Polyhedron*. 2018;150:83–91.
32. Kaltzoglou A, Manolis GK, Elsenety MM, et al. Synthesis and characterization of lead-free (CH3)3SSnI3 1-D perovskite. *J Electron Mater*. 2019;48:7533–7538.
33. Elsenety MM, Antoniadou M, Kaltzoglou A, et al. Synthesis, characterization of ((CH3)3S)2SnI6-nCln and ((CH3)3S)2SnI6-nBrn (n=1, 2) perovskites and use in dye-sensitized solar cells. *Mater Chem Phys*. 2020;239:122310.
34. Mekkey SD, Sultan ME, Elsenety MM, Helal A, Elsayed BA. Photocatalytic degradation of rhodamine B in the visible region using nanostructured CoAl2–xLaxO4 (x=0, 0.01, 0.03, 0.07, and 0.09) series: photocatalytic activity and DFT calculations. *Inorg Chem Commun*. 2022;136:109176.
35. Sobhy S, Elsenety MM, Mohamed MBI, Moustafa YM, Salama TM. Molecular dynamic simulations for interactions of oxytetracycline with copper(II)-exchanged NaY zeolite. *Inorg Chem Commun*. 2022;144:109829.
36. Gomaa H, Emran MY, Elsenety MM, et al. Selective removal of thorium ions from aqueous solutions using a hybrid mesoporous adsorbent as benzenesulfonamide-derivative @ ZrO 2. *J Water Process Eng*. 2023;51:103436.
37. Kaltzoglou A, Elsenety MM, Koutselas I, et al. Synthesis, characterization and optoelectronic properties of chemically stable (CH3)3SPbI3–xBrx and (CH3)3SPbI3–xClx (x= 0, 1, 2, 3) perovskites. *Polyhedron*. 2018;140:67–73.
38. Narayan H, Alemu H, Iwuoha E. Synthesis, characterization and conductivity measurements of polyaniline and poly aniline/fly-ash composites. *Phys Stat Sol (A) Appl Mater Sci*. 2006; 203:3665–3672.

39. Elsenety MM, Elsayed BA, Ibrahem IA, Bedair MA. Photophysical, DFT and molecular docking studies of Sm(III) and Eu(III) complexes of newly synthesized coumarin ligand. *Inorg Chem Commun*. 2020;121:108213.
40. Liu Y, Lee JY, Hong L. Morphology, crystallinity, and electrochemical properties of in situ formed poly(ethylene oxide)/TiO2 nanocomposite polymer electrolytes. *J Appl Polym Sci*. 2003;89:2815−2822.
41. Su SJ, Kuramoto N. Processable polyaniline−titanium dioxide nanocomposites: effect of titanium dioxide on the conductivity. *Synth Met*. 2000;114:147−153.
42. Gilja V, Novaković K, Travas-Sejdic J, Hrnjak-Murgić Z, Roković MK, Žic M. Stability and synergistic effect of polyaniline/TiO2 photocatalysts in degradation of Azo dye in wastewater. *Nanomaterials*. 2017;7:412−428.
43. Choi HJ, Kim MS, Ahn D, Yeo SY, Lee S. Electrical percolation threshold of carbon black in a polymer matrix and its application to antistatic fibre. *Sci Rep 2019*. 2019;9:1−12, 1. 9.
44. Huang WF, Xiao YL, Huang ZJ, Tsui GCP, Yeung KW, Tang CY, Liu Q. Super-hydrophobic polyaniline-TiO_2 hierarchical nanocomposite as anticorrosion coating. *Elsevier*; 2020 (n.d.) https://www.sciencedirect.com/science/article/pii/S0167577X19314533. Accessed March 12, 2023.
45. Al-Sabagh AM, Abdou MI, Migahed MA, et al. Influence of ilmenite ore particles as pigment on the anticorrosion and mechanical performance properties of polyamine cured epoxy for internal coating of gas transmission pipelines. *Egypt J Petrol*. 2018;27:427−436.
46. Al-Sabagh AM, Abdou MI, Migahed MA, Abd-Elwanees S, Fadl AM, Deiab A. Investigations using potentiodynamic polarization measurements, cure durability, ultra violet immovability and abrasion resistance of polyamine cured ilmenite epoxy coating for oil and gas storage steel tanks in petroleum sector. *Egypt J Petrol*. 2018;27:415−425.
47. Diantoro M, Masrul MZ, Taufiq A. Effect of TiO_2 nanoparticles on conductivity and thermal stability of PANI-TiO_2/glass composite film. *J Phys Conf Ser*. 2018;1011:012065−012071.
48. Pang AL, Arsad A, Ahmadipour M. Synthesis and factor affecting on the conductivity of polypyrrole: a short review. *Polym Adv Technol*. 2021;32:1428−1454.
49. Miyanishi S, Miyanishi S, Yamaguchi T, Yamaguchi T. Highly conductive mechanically robust high M w polyfluorene anion exchange membrane for alkaline fuel cell and water electrolysis application. *Polym Chem*. 2020;11:3812−3820.
50. Malhotra BD, Kumar N, Ghosh S, Singh HK, Chandra S. Poly-α-naphthalene oxide-pyrrole: a new electro-chemically-generated conducting polymer,. *Synth Met*. 1989;31:155−162.
51. Bekkar F, Bettahar F, Moreno I, et al. Synthesis and applications. A review of the last 10 Years,. *Polymers*. 2020;12:1−33.
52. Mudila H, Prasher P, Kumar M, Kumar A, Zaidi MGH, Kumar A. Critical analysis of polyindole and its composites in supercapacitor application. *Mater Renew Sustain Energy*. 2019;8:1−19.
53. Skotheim T. *Handbook of conducting polymers*. 1997.
54. Radoičić M, Ćirić-Marjanović G, Miličević D, et al. Fine-tuning of conductive and dielectric properties of polypyrrole/TiO2 nanocomposite-coated polyamide fabric. *Compos Interfac*. 2021;28:795−808.